International Journal of Applied Earth Observation and Geoinformation 54 (2017) 38–52

Contents lists available at ScienceDirect

International Journal of Applied Earth Observation and Geoinformation

journal homepage: www.elsevier.com/locate/jag

Defining optimal DEM resolutions and point densities for modelling hydrologically sensitive areas in agricultural catchments dominated by microtopography

I.A. Thomas[a,b,*], P. Jordan[a,b], O. Shine[a], O. Fenton[c], P.-E. Mellander[a], P. Dunlop[b], P.N.C. Murphy[d,e]

[a] Agricultural Catchments Programme, Teagasc, Johnstown Castle, Wexford, Co. Wexford, Ireland
[b] School of Geography and Environmental Sciences, Ulster University, Coleraine, Northern Ireland, United Kingdom
[c] Teagasc, Environmental Research Centre, Johnstown Castle, Wexford, Co. Wexford, Ireland
[d] Environment and Sustainable Resource Management Section, School of Agriculture and Food Science, University College Dublin, Dublin 4, Ireland
[e] University College Dublin Earth Institute, University College Dublin, Belfield, Dublin 4, Ireland

ARTICLE INFO

Article history:
Received 4 April 2016
Received in revised form 13 August 2016
Accepted 31 August 2016
Available online 16 September 2016

Keywords:
Diffuse pollution
Surface runoff
Microtopography
Critical source area
LiDAR
DEM

ABSTRACT

Defining critical source areas (CSAs) of diffuse pollution in agricultural catchments depends upon the accurate delineation of hydrologically sensitive areas (HSAs) at highest risk of generating surface runoff pathways. In topographically complex landscapes, this delineation is constrained by digital elevation model (DEM) resolution and the influence of microtopographic features. To address this, optimal DEM resolutions and point densities for spatially modelling HSAs were investigated, for onward use in delineating CSAs. The surface runoff framework was modelled using the Topographic Wetness Index (TWI) and maps were derived from 0.25 m LiDAR DEMs (40 bare-earth points m^{-2}), resampled 1 m and 2 m LiDAR DEMs, and a radar generated 5 m DEM. Furthermore, the resampled 1 m and 2 m LiDAR DEMs were regenerated with reduced bare-earth point densities (5, 2, 1, 0.5, 0.25 and 0.125 points m^{-2}) to analyse effects on elevation accuracy and important microtopographic features. Results were compared to surface runoff field observations in two 10 km^2 agricultural catchments for evaluation. Analysis showed that the accuracy of modelled HSAs using different thresholds (5%, 10% and 15% of the catchment area with the highest TWI values) was much higher using LiDAR data compared to the 5 m DEM (70–100% and 10–84%, respectively). This was attributed to the DEM capturing microtopographic features such as hedgerow banks, roads, tramlines and open agricultural drains, which acted as topographic barriers or channels that diverted runoff away from the hillslope scale flow direction. Furthermore, the identification of 'breakthrough' and 'delivery' points along runoff pathways where runoff and mobilised pollutants could be potentially transported between fields or delivered to the drainage channel network was much higher using LiDAR data compared to the 5 m DEM (75–100% and 0–100%, respectively). Optimal DEM resolutions of 1–2 m were identified for modelling HSAs, which balanced the need for microtopographic detail as well as surface generalisations required to model the natural hillslope scale movement of flow. Little loss of vertical accuracy was observed in 1–2 m LiDAR DEMs with reduced bare-earth point densities of 2–5 points m^{-2}, even at hedgerows. Further improvements in HSA models could be achieved if soil hydrological properties and the effects of flow sinks (filtered out in TWI models) on hydrological connectivity are also considered.

1. Introduction

Agricultural catchment areas at highest risk of diffuse pollution transfers are termed critical source areas (CSAs) (Doody et al., 2012). These are where large, mobile pollutant sources coincide with hydrologically sensitive areas (HSAs) at highest propensity for surface runoff generation, pollutant transport and delivery via

* Corresponding author at: Agricultural Catchments Programme, Teagasc, Johnstown Castle, Wexford, Co. Wexford, Ireland.
E-mail addresses: ianathomas@hotmail.co.uk, ian.thomas@teagasc.ie (I.A. Thomas), p.jordan@ulster.ac.uk (P. Jordan), oliver.shine@teagasc.ie (O. Shine), owen.fenton@teagasc.ie (O. Fenton), erik.mellander@teagasc.ie (P.-E. Mellander), p.dunlop@ulster.ac.uk (P. Dunlop), paul.murphy@ucd.ie (P.N.C. Murphy).

http://dx.doi.org/10.1016/j.jag.2016.08.012

hydrologically connected pathways (Gburek and Sharpley, 1998; Pionke et al., 2000; Walter et al., 2000). If agricultural pressures on water quality are to be minimised, HSAs and CSAs need to be modelled more accurately in order to target mitigation measures and best management practices at appropriate locations and scales (Sharpley et al., 2000; Sonneveld et al., 2006).

As topography is a dominant factor controlling surface runoff generation, HSAs can be modelled within a topographic framework such as the Topographic Wetness Index (TWI) by Beven and Kirkby (1979). The TWI estimates the relative propensity of a point in the landscape to become saturated and hence generate runoff based on the assumption that topography controls the near surface position of the groundwater table (Beven, 2001; Moore et al., 1991). The TWI uses topographic attributes derived from Digital Elevation Models (DEMs), and is defined as $\ln(\alpha/\tan\beta)$, where α (m) is the specific upslope drainage area per unit contour length and $\tan\beta$ (radians) is the local surface slope. Larger upslope drainage areas and shallower slopes will produce larger TWI values, indicating higher propensity for runoff (Quinn et al., 1991). Hydrological models (e.g. Lyon et al., 2004; Schneiderman et al., 2007; Archibald et al., 2014; Agnew et al., 2006), fate-and-transport models such as SWAT-VSA (Collick et al., 2014; Easton et al., 2008) and CSA indices (Marjerison et al., 2011; Buchanan et al., 2013a) use topographic indices such as the TWI as a framework to model HSAs, runoff pathways and pollutant transport risk.

However, the TWI is sensitive to DEM grid resolution, because it affects both terrain representation and the topographic attributes used within the index (Zhang and Montgomery, 1994; Kienzle, 2004). Coarser DEM resolutions tend to produce narrower slope distributions and lower mean slope gradients, attributed to the smoothing of topography and loss of topographic detail, with lower gradients on steeper slopes and higher gradients on shallower slopes (Chang and Tsai, 1991; Thompson et al., 2001). Larger mean α values are also computed, attributed to less irregular flow paths and larger minimum areal units, with larger α values in upper landscape positions and lower α values in lower landscape positions (Thompson et al., 2001; Wu et al., 2008). Larger mean TWI values are therefore computed from coarser resolution DEMs, primarily due to the influence of α distributions rather than slope (Gillin et al., 2015; Sørensen and Seibert, 2007).

The optimal DEM resolution for deriving topographic indices depends on the hydrological process being modelled and the scale of the topographic features controlling it (Quinn et al., 1991; Chou et al., 1999). If a DEM is too coarse to capture or adequately represent the topographic features due to surface generalisations of the terrain, topographic index predictions might be erroneous (Hancock, 2005; Vaze et al., 2010). However, a very high DEM resolution may also be inappropriate (Kuo et al., 1999). For example, groundwater flow directions typically follow the general topography of the landscape rather than small-scale surface variations, and thus smoother topography represented in coarser resolutions may better represent near-surface flow pathways and water table positions (Gillin et al., 2015; Wolock and Price, 1994). The optimal DEM resolution therefore achieves a balance between appropriate levels of topographic accuracy, data processing and storage requirements, and the need for interpretable outputs (Liu, 2008; MacMillan et al., 2003; Hengl, 2006).

Microtopographic features, often anthropogenic and at sub-metre scale, can be prevalent in agricultural catchments, and influence diffuse pathways of surface runoff that can entrain pollutants (Buchanan et al., 2013a; Lane et al., 2009). Roads, tracks, tramlines and open agricultural drainage channels (ditches) can significantly increase hydrological connectivity and associated pollution delivery, by intercepting and concentrating significant quantities of surface runoff towards receiving waters (Bracken and Croke, 2007; Duke et al., 2003; Heathwaite et al., 2005; Shore et al., 2013). Other features such as hedgerow banks and local flow sinks (pits and depressions) can impede and/or divert runoff away from its natural flow path. Microtopographic features therefore play important roles in delineating HSAs and CSAs in agricultural catchments (Thomas et al., 2016; Buchanan et al., 2013b; Sherriff et al., 2015; Srinivasan and Mcdowell, 2009).

Coarser scale DEM resolutions (and point densities) may not capture microtopographic controls on HSAs and pathways, which limit their utility for identifying CSAs at small scales (Sharpley et al., 2002, 2011; Page et al., 2005). However, Light Detection and Ranging (LiDAR) technology allows the generation of high elevation point cloud densities and sub-metre resolution DEMs with high vertical accuracy over large spatial areas (Murphy et al., 2008; Luscombe et al., 2015). Furthermore, significant reductions in initial survey point densities may still allow highly accurate DEMs to be generated but with subsequent improvements in data storage and processing times (Brubaker et al., 2013; Anderson et al., 2006). LiDAR DEMs could therefore offer significant improvements in modelling HSAs and CSAs at sub-field scales and targeting management strategies to reduce diffuse pollution (Thomas et al., 2016; Djodjic and Villa, 2015; Galzki et al., 2011; Sharpley et al., 2015).

This study aimed to identify an optimal DEM resolution and point density for modelling HSAs in topographically complex agricultural landscapes dominated by microtopographic features, for onward use in CSA modelling at field and sub-field scales. The objectives were to; (a) compare the TWI and its components derived from a series of DEM products, including high resolution LiDAR, (b) model HSAs using the TWI at the different DEM resolutions and evaluate (ground truth) the HSA maps using field observations of surface runoff to identify an optimal resolution, and (c) identify a reduced point density appropriate for the optimal DEM resolution that minimises vertical error and oversampling.

2. Materials and methods

2.1. Study catchments

The study was undertaken in two headwater agricultural catchments in south-east Ireland (Fig. 1), named Arable A and Grassland B in Wall et al. (2011). Extensive catchment details are described in Mellander et al. (2012), Jordan et al. (2012) and Shore et al. (2013) and summaries are provided here.

Arable A is a predominantly arable catchment with well-drained soils (72% Brown Earths) and mainly subsurface hydrological pathways, although (transient) surface runoff pathways exist during storms (Mellander et al., 2015). Grassland B is a predominantly grassland catchment with poorly drained soils (71% Gleys) and flow pathways are dominated by surface runoff. Annual phosphorus (P) losses in Grassland B are an order of magnitude greater than in Arable A, despite similar annual rainfall (approximately 1000 mm) and lower soil P concentrations (Jordan et al., 2012; Shore et al., 2014), reflecting differences in soil permeability and dominant flow pathways rather than land use or intensity (Mellander et al., 2015). Both catchments have small field sizes (3 ha average), a mixture of concave and convex hillslope topography, and microtopography such as hedgerow banks, open drains, roads, tracks, ditches, pits/depressions, tramlines, culverts and bridges are prevalent throughout.

2.2. DEM datasets and processing

For each catchment, bare-earth 0.25 m resolution LiDAR DEMs (Supplementary Fig. S1 in the online version at DOI: http://dx.doi.org/10.1016/j.jag.2016.08.012) were obtained from aerial surveys commissioned in the winter of 2011-12, with average bare-earth point densities of 40 and 44 points m^{-2} and vertical and horizontal

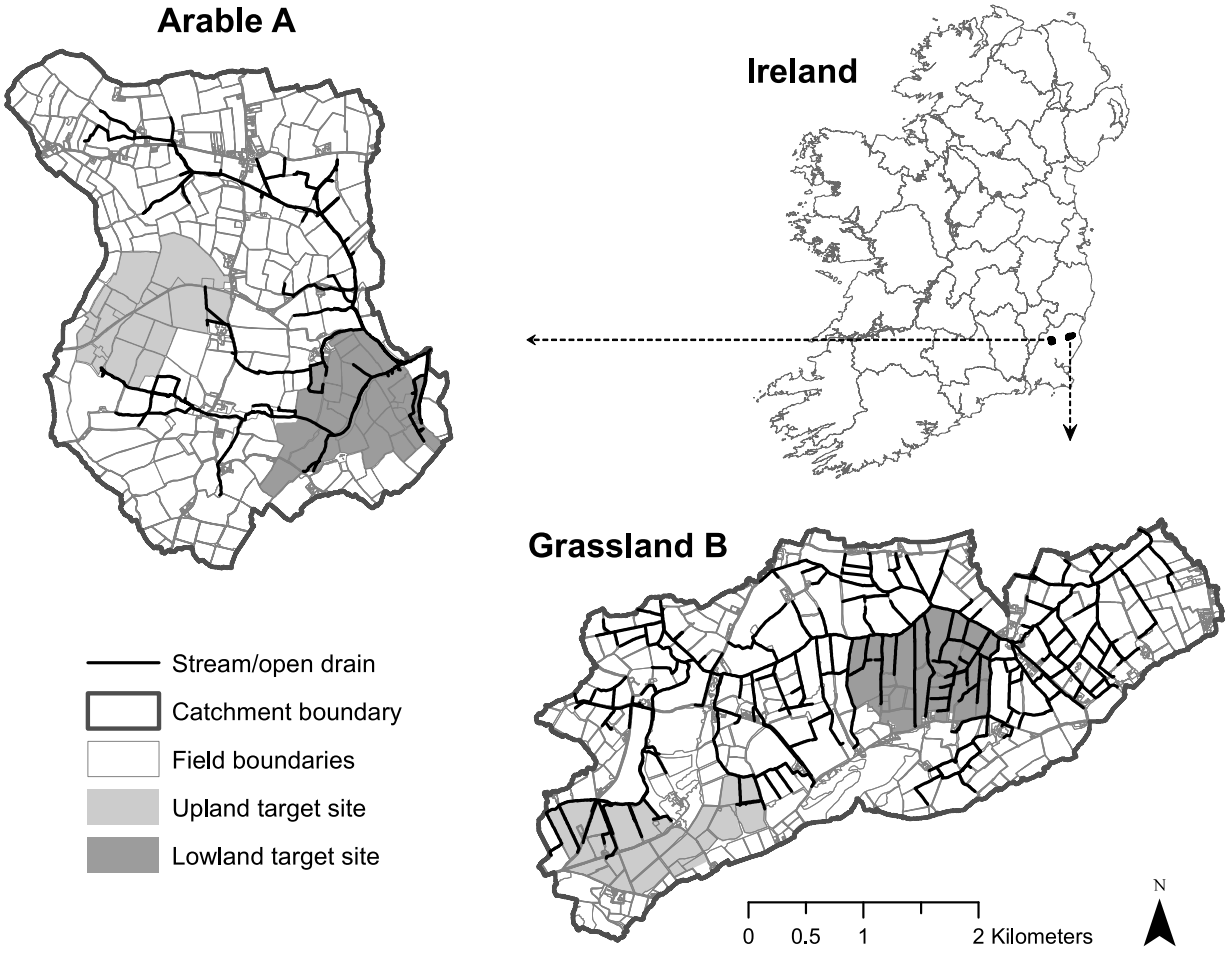

Fig. 1. Locations of Arable A and Grassland B catchments (and target sites) in Co. Wexford, Ireland.

accuracies of 0.15 m and 0.25 m respectively. Proprietary Intermap 5 m resolution DEMs (bare-earth NEXTMap Type II+ v1.5) derived from interferometric synthetic aperture radar (IFSAR) were also obtained, with vertical and horizontal accuracies of 1 m and 2 m respectively. LiDAR DEMs were pre-processed in ArcGIS v10.0 to remove local topographic noise caused by low vertical accuracy relative to horizontal sampling distance, and then resampled to 1 m and 2 m resolutions (Fig. 2). The TWI could therefore be computed at four grid resolutions, derived from 0.25 m, 1 m and 2 m LiDAR DEMs and a conventional 5 m DEM.

All DEMs were hydrologically corrected in SAGA GIS v.2.1 prior to computing the TWI to ensure drainage channel networks were accurate and fully connected (Fig. 2). A rasterised field-mapped stream network was 'burned' into the 5 m DEM using the stream burning tool, which decreases overlayed cell elevations by a defined value (10 m in this study). For LiDAR DEMs, which captured the stream network in fine detail, only field-mapped culverts, bridges and road drains (which represent artificial dams to modelled flow pathways) were burned. To create depressionless, fully connected DEMs for modelling flow pathways, flow sinks (pits and depressions) were identified and filled using the method by Wang and Liu (2006) which is computationally efficient and designed for large, high resolution LiDAR datasets. A minimum slope gradient between neighbouring cells of 0.1° was enforced.

2.3. Computation and analysis of the TWI

For all four resolutions, a slope raster grid was computed from the un-hydrologically corrected version of the DEM using the 'Fit 2. Degree Polynom' method by Zevenbergen and Thorne (1987) in SAGA GIS. The Deterministic Infinity ($D\infty$) method by Tarboton (1997) was applied to the hydrologically corrected DEM version to model multiple flow directions and calculate upslope drainage areas (flow accumulations). Upslope drainage areas were then converted to α by dividing values by the grid cell width in the grid calculator tool. Slope and α grids were then used as inputs in the TWI tool in SAGA GIS to derive a TWI map for each grid resolution.

Target sites were identified within each catchment to analyse TWI and component grids at hillslope scales, and to collect field observations for evaluating modelled HSAs. Sites were located in both upland and lowland areas (see Fig. 1) to reflect expected differences in soil saturation potential and slope distributions at different elevations, and targeted where microtopographic features existed. Thus, the effects of varying topographic information between DEM resolutions could be analysed.

Field, road and target site boundaries were digitised in ArcGIS, and catchment boundaries were delineated using the TauDEM (Terrain Analysis Using Digital Elevation Models) toolbox v5.1.1. All boundaries were rasterised at each of the four grid resolutions and used as zones in the zonal statistics tool to compute TWI and component summary statistics and frequency distributions.

2.4. Modelling HSAs and evaluating maps

For each grid resolution, TWI values were divided into 100 classes of equal area using the ArcGIS slice tool with equal area method. The highest class represented the 1% of the catchment area with the highest TWI values (runoff propensity). Arbitrary thresh-

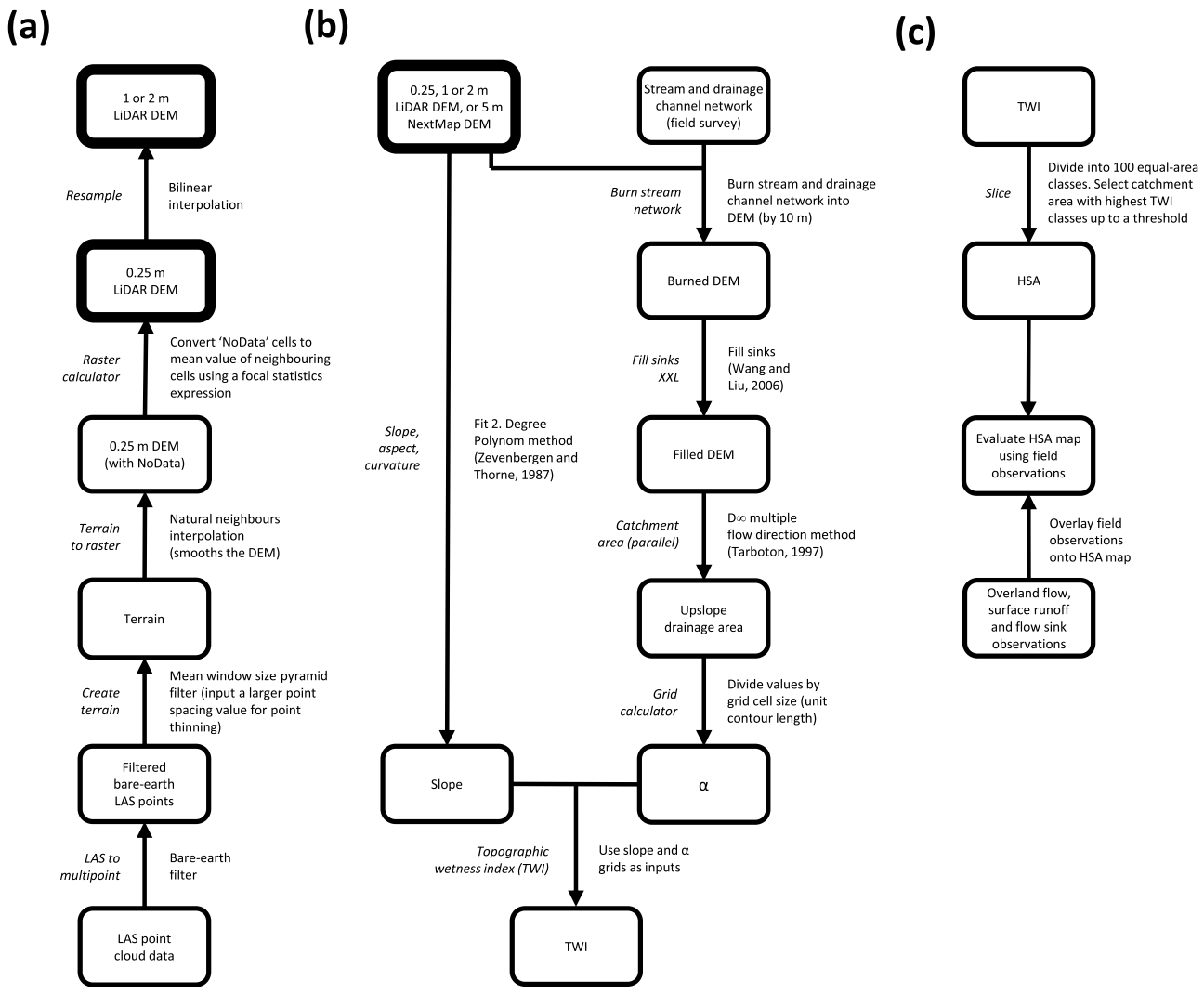

Fig. 2. Workflow showing (a) pre-processing and resampling of LiDAR DEMs in ArcGIS, (b) computation of TWI maps for each DEM resolution in SAGA GIS, and (c) delineation of HSAs and evaluation of HSA maps using field observations of overland flow, surface runoff and field boundary flow sinks. Also indicated are the tools (in italics on left) and methods (on right) used in each workflow process. DEMs are in bold.

olds (5%, 10% and 15% of the catchment area with the highest TWI values) were used to model HSAs. Multiple thresholds were used due to the risk of a given threshold over- or under-estimating the size of the HSA.

To evaluate modelled HSAs, field evidence of surface runoff was mapped at target sites. Observations were recorded during (and immediately after) large winter storm events which occurred following prolonged heavy rainfall, when saturation-excess overland flow generation would be greatest (Table 1). Due to the flashy nature of runoff events and the number of fields within target sites, only visual estimates were recorded. Observations included the approximate sub-field areas where overland flow and surface runoff occurred, pathways to the drainage channel network, and locations where pathways crossed a field or road boundary (termed breakthrough points) or were delivered to the drainage channel network (termed delivery points). Locations at field boundaries where overland flow pathways became impeded by a hedgerow bank, pit or depression (termed field boundary sinks) were also recorded. Field observations over multiple storm events were required for complete coverage of target sites. However, the small number of storms during the study period prevented observations being recorded in the lowland site of Grassland B. More survey time was given to Arable A as it experiences more transient surface runoff generation.

For each threshold, modelled HSAs were overlaid with field observations for evaluation. The number of observations that were intersected and hence correctly predicted were recorded, as well as those that did not intersect and were not predicted. Modelled breakthrough or delivery points within 20 m of observations were tolerated to account for potential spatial inaccuracies of the visual observations. As the DEMs were hydrologically corrected to accurately model subsurface flow direction and accumulation, any field boundary sinks had been removed, and to account for this, a breakthrough point modelled in the same location as an observed field boundary sink (with a 20 m tolerance) was counted as a correct prediction.

2.5. Effects of LiDAR point density reductions on DEM elevation

The effects of LiDAR point density reductions on DEM elevations were analysed at the catchment scale and at microtopographic features (hedgerow banks) within target sites for Arable A. The raw LiDAR bare-earth point cloud dataset (40 points m^{-2}) was thinned during the terrain pyramid building process in ArcGIS (see Fig. 2) using different sample window sizes (point spacings) of 0.45, 0.71,

Table 1
Storm events used for field observations of surface runoff at target sites. Antecedent rainfall is also indicated.

Storm event	Catchment	Target site	Time period of event	Time period of observations	Total rainfall (mm)	Total rainfall in previous 24 h (mm)	Total rainfall in previous 2 weeks (mm)	Fields observed
31/01/14	Arable A	Upland	03:00–12:00	08:30–12:15	15.2	1.6	59.2	19/19
03/02/14	Arable A	Lowland	05:00–11:00	09:00–11:45	8.4	0.2	76.2	14/31
12/02/14	Arable A	Lowland	05:00–10:00	09:00–10:45	13.2	0.2	90.2	5/31
25/02/14	Grassland B	Upland	07:00–10:00	08:00–12:00	1	11.4	87.8	14/25

1.0, 1.41, 2.0, 2.83 and 8 m, to generate a series of 1 m and 2 m DEMs with reduced point densities of 5, 2, 1, 0.5, 0.25, 0.125 and 0.0156 points m^{-2}, respectively. For a defined sample window size, the lowest elevation point within the sample window was selected, to represent the worst-case scenario in terms of capturing positive or high elevation features such as hedgerow banks or other flow-diverting microtopographic barriers in the landscape. Absolute differences in elevations (in metres) between the un-thinned DEM and thinned DEMs were then calculated for both 1 m and 2 m grid resolutions.

3. Results

3.1. Effects of microtopographic information on TWI and component grids

Microtopographic features were captured within all LiDAR DEMs (Fig. 3). However, features became less well defined at coarser LiDAR resolutions. Bridges and higher-order stream channels were the only microtopographic features captured within 5 m DEMs.

The variation in topographic information contained within each DEM had significant effects on the spatial distributions of slope, α and TWI values (Fig. 4). Higher slope values were computed at microtopographic features in LiDAR resolutions. Therefore, although modelled surface flow pathways tended to follow hillslope scale topography at all resolutions, hedgerow banks, roads, tracks and tramlines acted as topographic barriers or channels that accumulated flow and diverted it away from its natural flow path until a gap in the feature was encountered (Fig. 5). Thus, the highest TWI values tended to be located where microtopographic features accumulated flow, and hillslope positions downslope of flow diversions computed low α and TWI values. These dynamics were not modelled at 5 m resolution. However, 1–5 m resolution TWI maps showed spatial similarities at lower hillslope positions, as similar α distributions were computed due to the control of hillslope scale topography. Coarser LiDAR resolutions captured microtopographic features in poorer detail which tended to produce a greater number of gaps and hence smaller flow diversions. Very high topographic variability and very low flow accumulations were shown in 0.25 m resolution slope and α grids. As in-field microtopography was prevalent at this resolution, general hillslope topography and landscape position indicated less influence on flow pathways and TWI values, and grids were also much less visually interpretable at this resolution.

Summary statistics and frequency distributions showed clear trends as resolutions increased. Finer resolution DEMs computed higher median slope values, lower median α and TWI values, and larger ranges of values at each catchment and target site (Tables 2 and 3). Standard deviations also tended to increase. Roads computed higher average and maximum α values (as they effectively accumulated flow from upslope fields), and hence higher maximum TWI values. Slope and TWI frequency distributions became broader and less symmetrically distributed, and α distributions became more positively skewed (Fig. 6). At 0.25 m resolution the majority of cells computed large slopes and very small α values. When analysis focused on within-field areas and hence excluded hedgerow banks and microtopography outside of field boundaries, average slope values decreased at each LiDAR resolution but remained constant at 5 m.

3.2. HSAs and field evaluation

For each TWI threshold, modelled HSAs became more spatially distributed at finer resolutions and extended into higher hillslope positions (Figs. 7 and 8). This was particularly evident at the finest resolution, which predicted high runoff propensity throughout every field. Runoff pathways in all LiDAR resolutions tended to be controlled by flow-diverting features, including hedgerow banks, roads, tracks and tramlines. Spatial similarities in lower hillslope positions were found at 1–5 m resolutions, where runoff often converged to the same location. HSAs were also modelled at every location known to have artificial subsurface drainage (five in Arable A and two in Grassland B).

Field observations recorded interception, accumulation and channelisation of surface flow from microtopographic features (Figs. 7 and 8, and Supplementary Figs. S2 and S3 in the online version at DOI: http://dx.doi.org/10.1016/j.jag.2016.08.012). Runoff (HSAs) occurred in 50% of observed fields in Arable A and in 79% of observed fields in Grassland B, and the longest runoff pathways were approximately 1.3 km and 0.8 km respectively. Breakthrough points occurred at gaps in hedgerow banks or at gateways. Field boundary sinks typically occurred in downslope locations on shallow slopes where hedgerow banks were fully intact and without gateways. Delivery points were found at both higher and lower order stream channels and at open agricultural drains.

For each target site, LiDAR resolutions modelled HSAs at much higher spatial accuracies compared to 5 m maps (Figs. 7 and 8). Using 5%, 10% and 15% catchment area thresholds, LiDAR derived TWI maps correctly predicted 70–100%, 75–100% and 85–100% of sub-field areas where surface runoff or overland flow was observed or had been evident, compared to 10–58%, 40–74% and 60–84% using 5 m TWI maps (Table 4). Observed breakthrough points, delivery points and field boundary sinks were predicted with 75–100% accuracy at the varying LiDAR resolutions and thresholds, compared to 0–100% accuracy at the 5 m resolution. For all DEM resolutions, modelled HSAs tended to extend further into upper hillslope positions than field observations. As 0.25 m resolutions over-predicted runoff risk by modelling high runoff propensity throughout every field (Figs. 7 and 8), the optimal DEM resolution for modelling HSAs based on the TWI thresholds was identified as 1–2 m.

3.3. Effects of reduced LiDAR point density on DEM elevation

Compared to the initial un-thinned LiDAR DEM (40 points m^{-2}), LIDAR bare-earth point densities of between 5 and 2 points m^{-2} produced DEMs with elevations largely unchanged, even at hedgerow bank features (Table 5). At the catchment scale, very small mean absolute differences were found, even at the lowest point densities. When analysis focused on hedgerow banks within target sites, mean differences remained very small at den-

Table 2
TWI and component summary statistics at each DEM grid resolution for Arable A catchment and target sites.

		Catchment				Target site																							
						Upland site				Upland site (within fields and roads only)				Upland site (within fields only)				Upland site (roads only)				Lowland site				Lowland site (within fields only)			
Grid resolution (m)		0.25	1	2	5	0.25	1	2	5	0.25	1	2	5	0.25	1	2	5	0.25	1	2	5	0.25	1	2	5	0.25	1	2	5
Slope (degrees)	Mean	5.8	4.7	4.4	3.6	5.7	4.8	4.6	4.2	5.0	4.3	4.3	4.2	5.0	4.3	4.3	4.2	3.2	3.1	4.3	4.5	5.5	4.3	4.0	3.1	4.1	3.2	3.2	3.0
	Median	4	3	3	3	5	4	3	3	4	3	3	3	4	3	3	3	3	2	3	4	4	3	3	3	4	3	3	3
	Min	0	0	0	0	0	0	0	0	0	0	0	0	0	0	0	0	0	0	0	2	0	0	0	0	0	0	0	0
	Max	86	74	57	22	80	62	50	17	70	48	34	17	70	48	34	17	51	34	34	9	80	64	53	14	62	45	31	13
	σ	6.3	5.0	3.9	2.4	5.3	4.4	3.7	2.5	3.1	2.7	2.8	4.2	3.1	2.7	2.8	2.5	2.0	2.5	4.0	1.6	6.4	5.1	4.0	1.8	2.8	2.0	2.1	1.7
α (m)	Mean	2679	2693	2606	2535	823	713	619	523	6.51	615	595	523	446	450	531	524	26964	21731	8822	411	4387	4539	4439	4578	403	415	439	906
	Median	0.25	37	56	120	0.25	56	92	205	0.25	61	98	203	0.25	62	98	203	0.25	8	142	245	0.25	29	43	83	0.25	33	47	82
	Min	0.25	1	2	5	0.25	1	2	5	0.25	1	2	5	0.25	1	2	5	0.25	1	2	24	0.25	1	2	5	0.25	1	2	5
	Max (k)	43757	10997	5514	2227	2667	586	265	111	2667	586	265	111	2667	586	265	111	2183	438	120	7	25583	6328	3167	1273	25583	6328	3167	1273
	σ (k)	156	90	66	42	28	12	6	3	22	10	6	3	17	8	5	3	170	65	18	0.7	197	118	85	55	46	29	22	25
TWI (value)	Mean	4.0	6.3	6.9	7.8	4.1	6.6	7.2	8.2	4.3	6.9	7.4	8.2	4.3	6.9	7.4	8.2	4.2	7.3	8.3	8.2	3.8	6.2	6.7	7.7	4.0	6.5	7.0	7.6
	Median	3	6	7	8	4	7	7	8	4	7	7	8	4	7	7	8	3	5	8	8	3	6	7	7	3	6	7	7
	Min	−3	0	0	3	−2	0	1	4	−1	0	1	4	−1	0	1	4	0	2	2	6	−2	0	1	4	−1	0	1	4
	Max	24	22	20	21	21	19	18	17	21	19	18	17	21	19	18	17	21	18	17	12	22	21	20	21	21	20	20	19
	σ	2.7	2.1	1.9	1.5	2.7	2.0	1.8	1.3	2.6	1.7	1.6	1.3	2.6	1.7	1.6	1.3	3.4	4.0	3.7	1.1	2.7	2.1	1.9	1.6	2.6	1.7	1.5	1.3

Table 3
TWI and component summary statistics at each DEM grid resolution for Grassland B catchment and target sites.

		Catchment				Target site																							
						Upland site				Upland site (within fields and roads only)				Upland site (within fields only)				Upland site (roads only)				Lowland site				Lowland site (within fields only)			
Grid resolution (m)		0.25	1	2	5	0.25	1	2	5	0.25	1	2	5	0.25	1	2	5	0.25	1	2	5	0.25	1	2	5	0.25	1	2	5
Slope (degrees)	Mean	6.9	5.2	4.6	3.3	8.6	7.5	7.1	6.5	7.6	6.7	6.6	6.6	7.6	6.7	6.6	6.6	5.1	5.0	6.3	6.6	5.5	4.0	3.5	2.2	4.0	2.9	2.8	2.3
	Median	4	3	3	2	7	7	7	7	7	7	7	7	7	7	7	7	4	4	4	7	4	3	3	2	4	3	3	2
	Min	0	0	0	0	0	0	0	0	0	0	0	0	0	0	0	0	0	0	0	1	0	0	0	0	0	0	0	0
	Max	87	82	76	38	80	64	49	19	72	48	31	19	67	38	28	19	72	48	31	13	82	60	44	10	59	43	28	10
	σ	8.1	6.6	5.2	3.6	6.7	5.3	4.3	3.1	4.2	3.3	3.3	3.1	4.2	3.3	3.3	3.1	4.4	4.7	5.2	2.6	6.8	5.3	3.5	1.5	2.4	1.8	1.8	1.5
α (m)	Mean	3791	3952	4022	3654	850	765	630	668	728	637	496	498	535	445	470	500	15844	15677	2519	384	768	814	759	705	452	396	449	363
	Median	0.25	11	22	66	4	46	83	246	8	54	92	246	8	54	92	245	0.25	53	90	314	0.25	9	15	58	0.25	11	17	55
	Min	0.25	1	2	5	0.25	1	2	5	0.25	1	2	5	0.25	1	2	5	0.25	1	2	5	0.25	1	2	5	0.25	1	2	5
	Max (k)	47157	11734	5914	2393	1133	281	165	217	1128	281	165	217	1128	281	83	217	997	273	165	19	1300	356	259	303	864	193	259	303
	σ (k)	244	139	113	68	18	8	4	4	16	7	2	3	11	4	2	3	100	50	8	1	16	9	6	4	11	4	4	3
TWI (value)	Mean	3.5	5.6	6.3	7.7	4.2	6.0	6.6	7.7	4.4	6.2	6.8	7.7	4.4	6.2	6.8	7.7	4.2	7.4	7.2	7.5	3.6	5.7	6.3	7.8	3.7	5.9	6.5	7.6
	Median	3	5	6	7	4	6	7	8	4	6	7	8	4	6	7	8	3	7	7	8	3	5	6	7	3	6	6	7
	Min	−3	−1	0	3	−2	0	1	4	−1	0	1	4	−1	0	1	4	−1	0	1	4	−2	0	1	4	−1	0	1	4
	Max	24	22	20	22	20	19	17	16	20	19	17	16	20	17	17	16	19	19	16	12	20	18	18	17	20	18	18	17
	σ	2.6	2.3	2.1	1.8	2.6	2.1	2.0	1.4	2.6	1.8	1.7	1.3	2.5	1.8	1.7	1.3	3.6	3.7	2.9	1.2	2.6	2.3	2.2	1.8	2.5	2.0	2.0	1.6

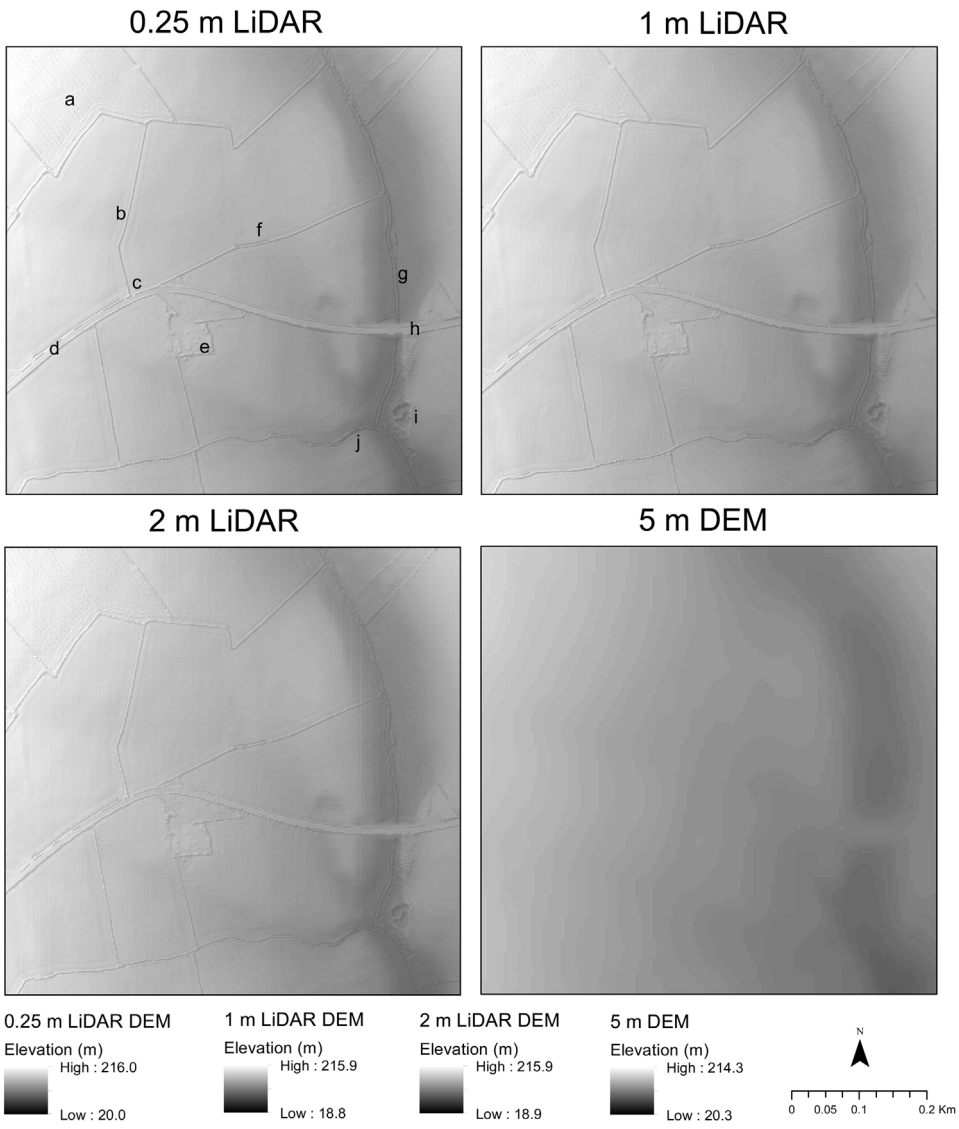

Fig. 3. Examples of microtopographic features captured in (hillshaded) LiDAR DEMs, including (a) tramlines, (b) hedgerow banks, (c) gateways, (d) roads, (e) buildings and yards, (f) open agricultural drains, (g) higher-order stream channels, (h) bridges, (i) hollows and (j) low-order stream channels. 5 m DEMs only captured bridges and higher-order stream channels. Darker colours represent lower elevations.

sities of 5 and 2 points m^{-2}, but markedly increased at densities of ≤ 1 point m^{-2}. Considering the height of these features typically ranged between 1–3 m, maximum differences were large within all thinned DEMs.

4. Discussion

4.1. TWI comparisons and optimal DEM resolutions

High resolution LiDAR and conventional resolution DEMs computed topographic indices that represented different scales of topographic control on surface hydrology as well as different forms of hydrological pathways. TWI maps derived from the 0.25 m LiDAR DEM predominantly captured the influence of microtopographic features (both artificial and natural) on flow and surface runoff pathways (Figs. 4 and 5). Conversely, 5 m TWI maps captured the natural hillslope scale movement of flow and surface runoff in the landscape, without artificial influences, and therefore also indicated general hillslope flow convergence.

Trends found in values and distributions of slope, α and TWI between resolutions (Tables 2, 3 and Fig. 6) build upon findings from other studies investigating the effects of high resolution LiDAR DEMs (e.g. Gillin et al., 2015; Sørensen and Seibert, 2007; Vaze et al., 2010). Significantly, 0.25 m LiDAR DEMs were found to be unsuitable for modelling topographic HSAs directly, due to the effects of very high topographic detail on flow accumulation. The majority of cells computed very small α values (0.25–10 m), attributed to rough terrain, larger slopes, smaller minimum areal units, and confinement of accumulated flow within very fine, single, irregular pathways. This resulted in much lower average TWI values and broader distributions compared to other resolutions. Therefore, the thresholds used to define HSAs (the 5%, 10% or 15% of the catchment area with the highest TWI values) included a larger range of TWI values found throughout most fields and hillslope positions, causing runoff risk to be over-predicted when compared to field observations (see Figs. 7 and 8). Thus topographic indices derived from finer resolution LiDAR DEMs are more controlled by microtopography, are less sensitive to landscape (hillslope) position, and compute wet areas (high values) further upslope, compared to coarser DEM resolutions (Murphy et al., 2009; Drover et al., 2015).

Resampling the 0.25 m LiDAR data to 1 and 2 m resolutions considerably improved predictions of surface runoff risk (Figs. 7 and 8).

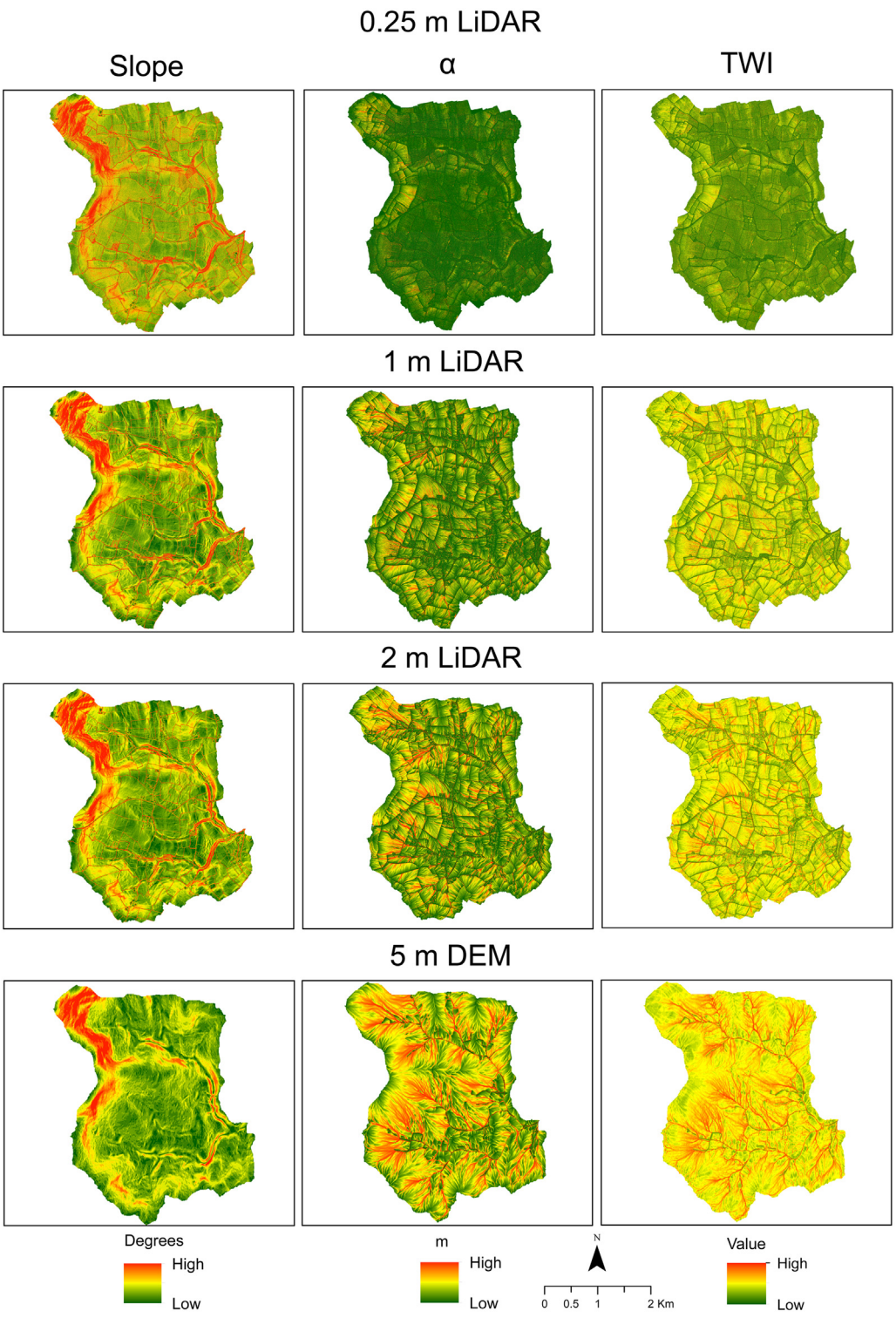

Fig. 4. TWI and component grids derived from each DEM resolution for Arable A.

The optimal DEM resolutions for modelling HSAs were therefore identified as 1–2 m because they were able to capture flow pathways controlled by both microtopography and hillslope convergence (landscape position). This was confirmed through field observations when compared to results from conventional 5 m DEMs (Table 4). These findings are also expected to apply to modifications of the TWI such as the Network Index (Lane et al., 2009) or soil topographic index (Walter et al., 2002), even if using a different multiple flow direction algorithm to that used in this study, because the effects on slope and hence flow accumulation would remain the same.

4.2. Implications for identifying and mitigating CSAs

The ability of LiDAR DEMs to accurately model breakthrough and delivery points allow CSA mitigation measures and agri-environment schemes to be considered at these critical locations of pollutant transfer, which could significantly improve cost-

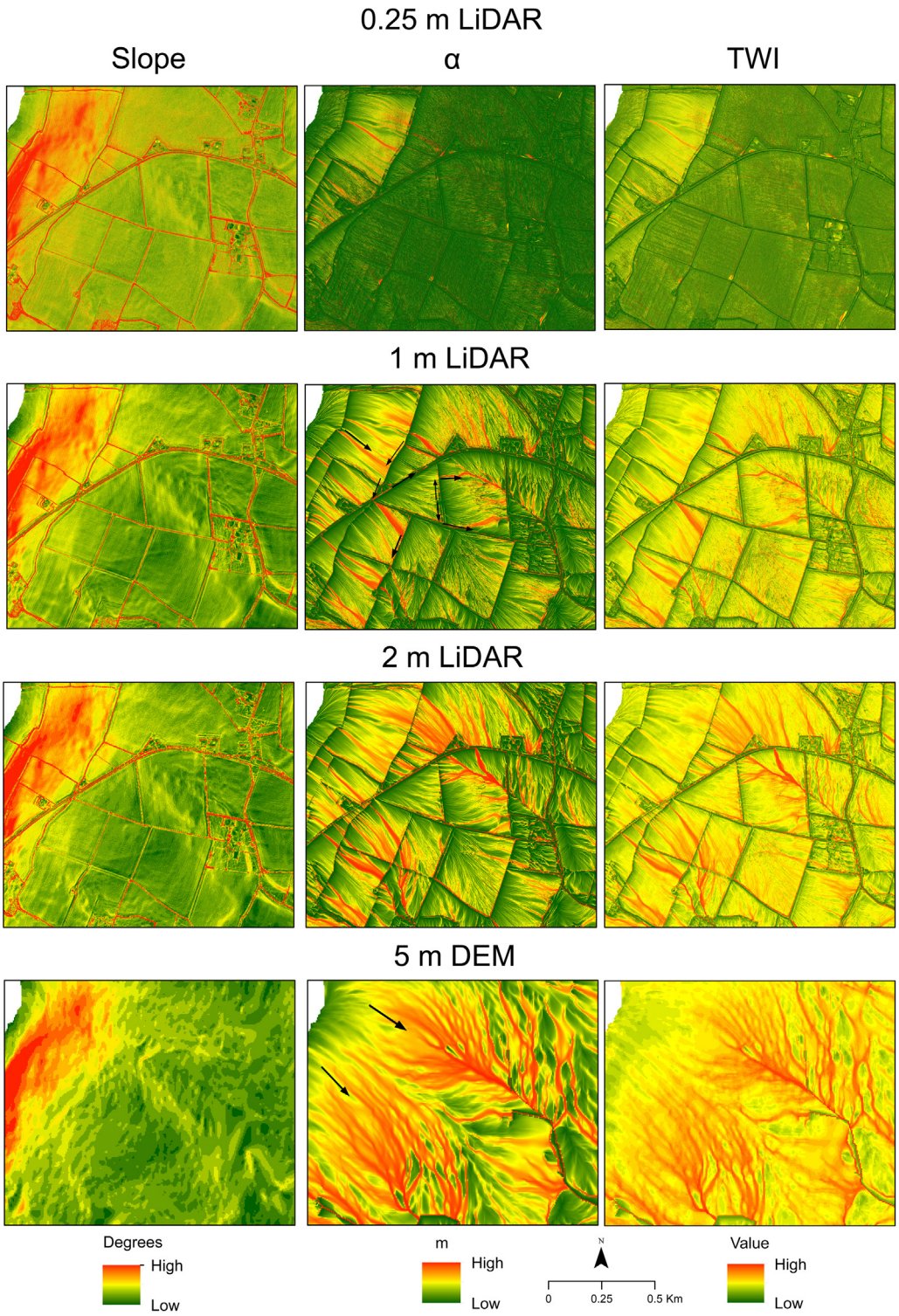

Fig. 5. Effects of microtopographic features on TWI and component grids. Flow directions in 1 m and 5 m α grids are indicated by arrows.

effectiveness (Doody et al., 2012). Conceptually, breakthrough points represent locations along surface runoff pathways (HSAs) in upper hillslope positions where mobilised pollutants are transferred between fields, whereas delivery points represent locations at the end of pathways in lower hillslope positions where transported pollutants could be delivered to the drainage channel network (Thomas et al., 2016). Targeting measures at breakthrough points would allow pollutants to be intercepted and trapped close to the source. The prevalence of hedgerow banks enhances mitigation potential as multiple runoff pathways are often confined within fields and channelled to a single breakthrough point such as a gateway. Measures could also be focused at the delivery points along the drainage channel network to reduce pollutant delivery, or at entire sections of the ditch and stream channels that have a high number of delivery points (indicating high hydrological risk of P

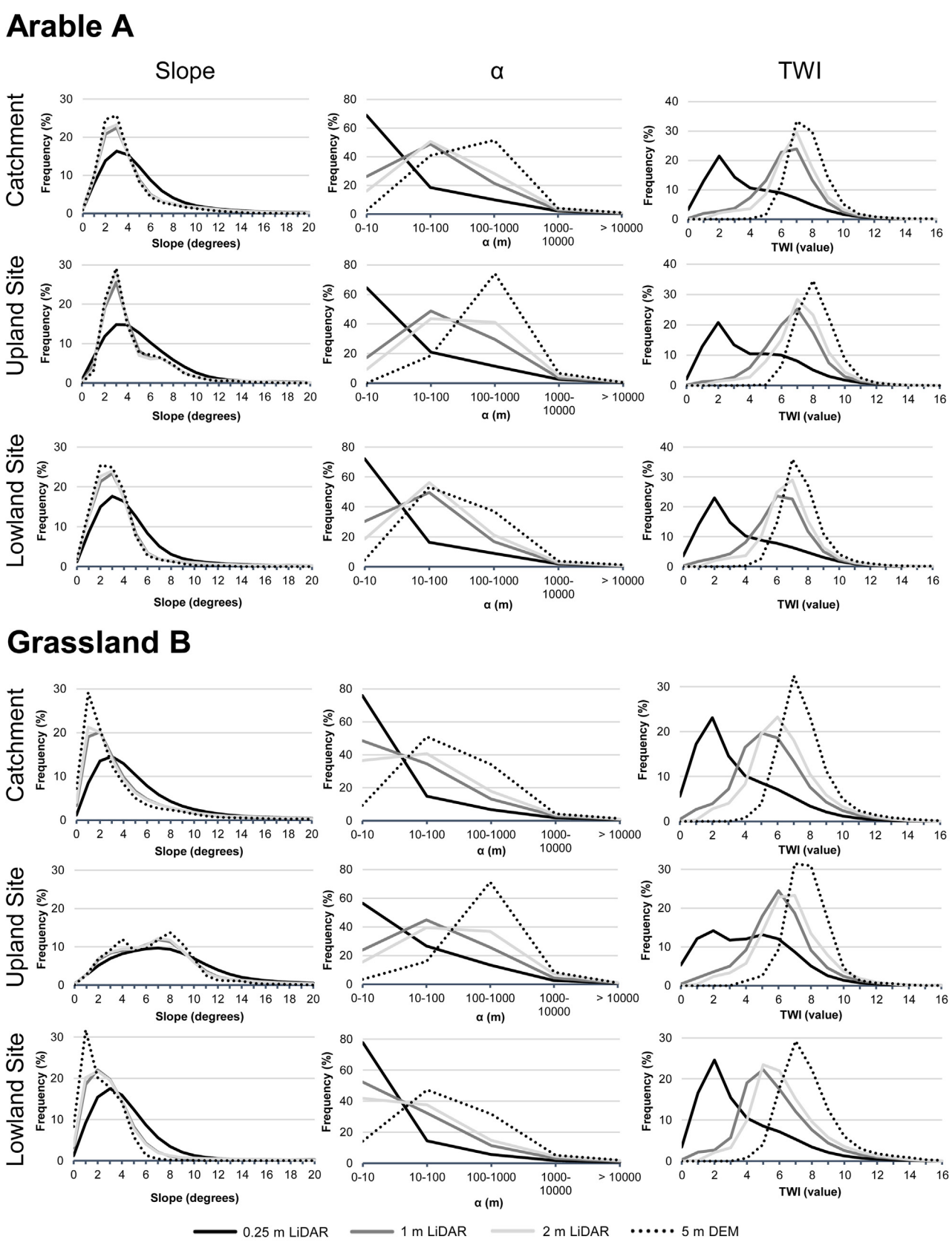

Fig. 6. Frequency distributions of the TWI and its components derived from each DEM resolution for each catchment and target site.

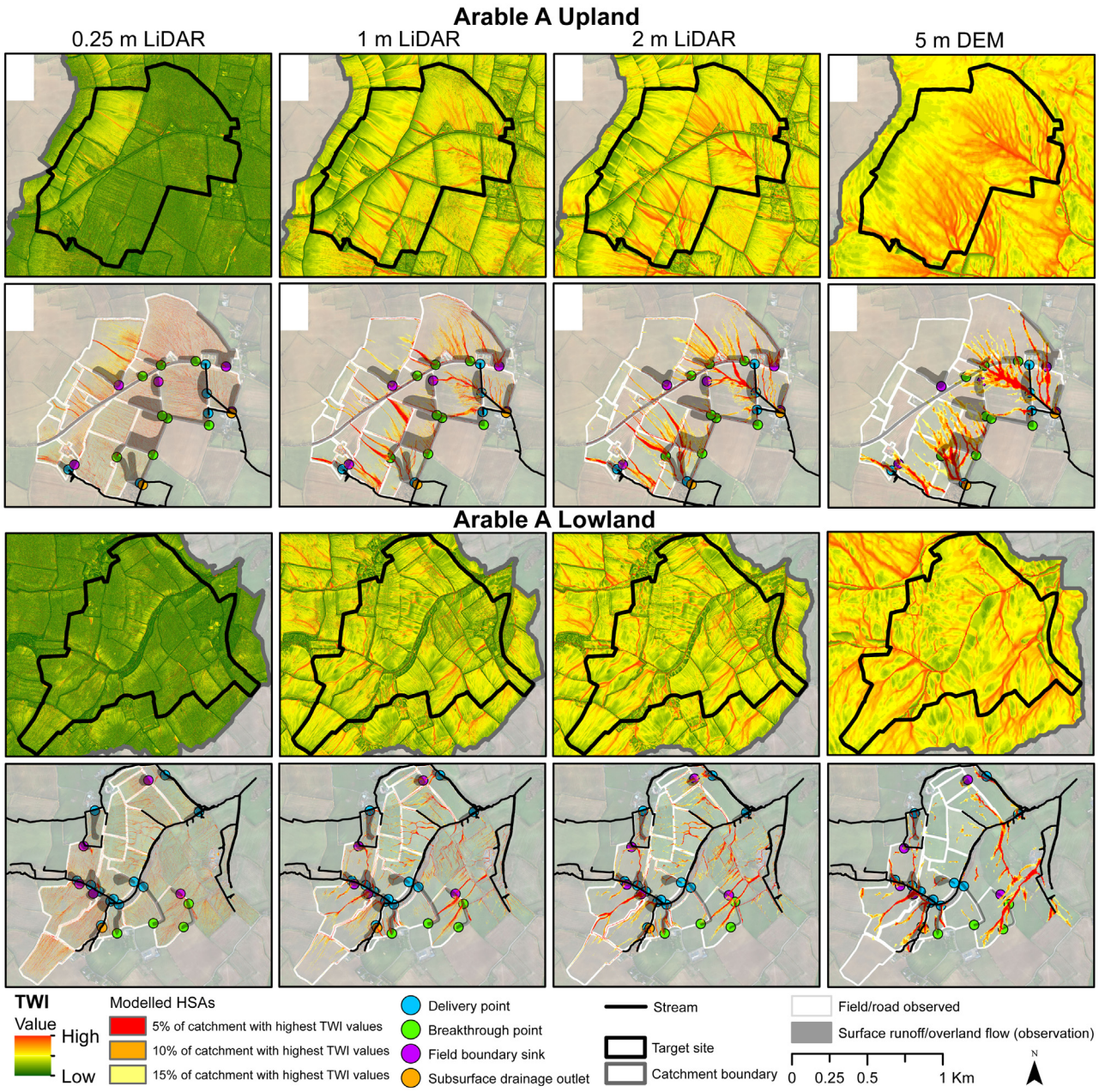

Fig. 7. TWI and HSA maps at each grid resolution for Arable A target sites, overlaid with field observations of surface runoff and overland flow, breakthrough points, delivery points and field boundary sinks.

delivery). Such high-precision, sub-field scale targeting of measures could not be implemented using coarser resolution DEMs.

4.3. Wider applicability of findings

In regions with similar complex microtopography, land use and climate (e.g. much of north-western Europe), the need for high resolution LiDAR DEMs for hydrological modelling and CSA mapping is becoming clear. This has been demonstrated in Swedish agricultural catchments for example, where rill and gully features have important controls on runoff, soil erosion and CSAs (Djodjic and Villa, 2015). In the USA, high resolution (3 m) LiDAR DEMs have been found to outperform 10 m and 30 m USGS DEMs for modelling soil moisture patterns, gullies and CSAs in agricultural catchments in New York and Minnesota (Buchanan et al., 2014; Galzki et al., 2011). Hydric soil mapping has also been improved in the Northern Appalachians using slopes and depressions computed from 1 m and 5 m LiDAR DEMs (Fink and Drohan, 2016).

However, the optimal DEM resolution for modelling HSAs and pollutant transport pathways will likely be landscape specific (Sørensen and Seibert, 2007; Murphy et al., 2009; Fink and Drohan, 2016). For example, in forested catchments in both the USA and Sweden, coarse DEM resolutions (ranging from 10 m to 50 m) were found to be optimal for modelling soil wetness, hydric soils, wetland vegetation and depths to groundwater (Drover et al., 2015; Tenenbaum et al., 2006; Ågren et al., 2014). This was due to deeper, more transmissive and undisturbed soils, dominant subsurface flow paths, steeper slopes, smoothing of noisy microtopographic detail such as tree mounds, and the shape of the terrain. It is therefore possible that coarser DEMs would also be more appropriate in agricultural catchments where microtopography does not dominate or exist.

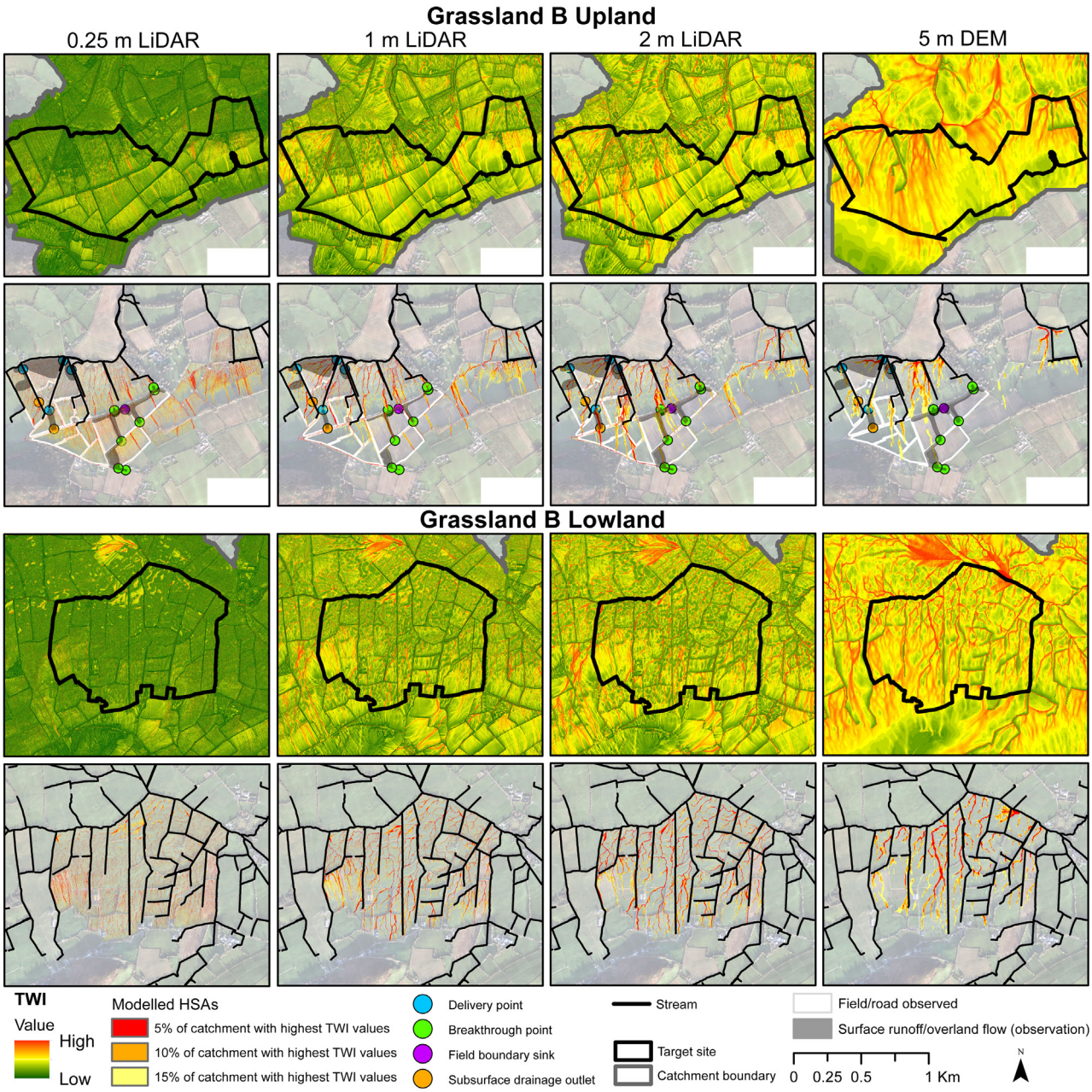

Fig. 8. TWI and HSA maps at each grid resolution for Grassland B target sites, overlaid with field observations of surface runoff and overland flow, breakthrough points, delivery points and field boundary sinks.

4.4. Optimal DEM point densities

Results show that in agricultural catchments of similar topographic complexity, significant point density reductions (from ~40 to 5 or 2 bare-earth points m^{-2}) could be achieved in future LiDAR surveys without loss of DEM elevation accuracy, even at microtopographic features (Table 5). This is partly attributed to both oversampling and raster interpolation, and similar findings have been shown by Brubaker et al. (2013), Anderson et al. (2006) and Raber et al. (2007). Such densities would require cheaper, less advanced LiDAR technologies, and would improve data storage and processing efficiency (Liu, 2008; Liu and Zhang, 2008). However, further research is warranted to analyse whether other hydrologically important microtopographic features, such as ditches, low-order stream channels and roads, are also well represented at lower survey point densities.

4.5. Other considerations

The modelled HSAs based only on TWI thresholds in this study tended to extend further into upper hillslope positions than field observations. This may in part be due to the TWI not capturing differences in soil properties and drainage classes between hillslope positions. For example, in Arable A, poorly drained soils (Groundwater Gleys) are predominantly found in lower hillslope positions and adjacent to the drainage channel network, whereas well drained soils dominate upslope (see Melland et al., 2012). Integrating topographic indices derived from optimal DEM resolutions with appropriate scale maps of soil hydrological properties such as permeability and depth (i.e. soil topographic indices) would be necessary to improve HSA modelling (Ali et al., 2014; Thomas et al., 2016; Mellander et al., 2015; Blyth et al., 2004).

Table 4
Percentage of surface runoff and overland flow field observations predicted using TWI-derived maps of HSAs for each threshold and grid resolution.

HSA threshold (% of catchment area with the highest TWI values)	Target site	Arable A								Grassland B			
		Upland				Lowland				Upland			
	Grid resolution (m)	0.25	1	2	5	0.25	1	2	5	0.25	1	2	5
		Sub-field areas generating surface runoff or overland flow											
	Total observed	19				20				10			
5%	Predicted	19	18	18	11	19	17	14	10	10	9	10	1
	Predicted (%)	100	95	95	58	95	85	70	50	100	90	100	10
10%	Predicted	19	18	18	14	20	19	15	13	10	9	10	4
	Predicted (%)	100	95	95	74	100	95	75	65	100	90	100	40
15%	Predicted	19	18	18	16	20	19	17	13	10	9	10	6
	Predicted (%)	100	95	95	84	100	95	85	65	100	90	100	60
		Breakthrough points											
	Total observed	8				4				8			
5%	Predicted	7	7	7	4	3	3	3	2	8	7	8	0
	Predicted (%)	87.5	87.5	87.5	50	75	75	75	50	100	87.5	100	0
10%	Predicted	7	7	7	4	3	3	3	2	8	8	8	0
	Predicted (%)	87.5	87.5	87.5	50	75	75	75	50	100	100	100	0
15%	Predicted	7	7	7	4	3	3	3	2	8	8	8	0
	Predicted (%)	87.5	87.5	87.5	50	75	75	75	50	100	100	100	0
		Delivery points											
	Total observed	5				12				4			
5%	Predicted	5	5	5	4	11	11	10	8	4	3	4	2
	Predicted (%)	100	100	100	80	91.7	91.7	83.3	66.7	100	75	100	50
10%	Predicted	5	5	5	4	11	11	11	8	4	3	4	3
	Predicted (%)	100	100	100	80	91.7	91.7	91.7	66.7	100	75	100	75
15%	Predicted	5	5	5	4	11	11	11	8	4	4	4	4
	Predicted (%)	100	100	100	80	91.7	91.7	91.7	66.7	100	100	100	100
		Field boundary sinks											
	Total observed	5				5				1			
5%	Predicted	5	5	5	3	5	5	5	2	1	1	1	0
	Predicted (%)	100	100	100	60	100	100	100	40	100	100	100	0
10%	Predicted	5	5	5	4	5	5	5	5	1	1	1	0
	Predicted (%)	100	100	100	80	100	100	100	100	100	100	100	0
15%	Predicted	5	5	5	4	5	5	5	5	1	1	1	0
	Predicted (%)	100	100	100	80	100	100	100	100	100	100	100	0

Table 5
Mean and maximum absolute differences in elevations (m) of LiDAR DEMs generated from different bare-earth point densities at the catchment scale and at hedgerow banks within target sites in Arable A.

			Absolute difference in elevation (m)							
			Mean				Maximum			
			1 m LiDAR DEM		2 m LiDAR DEM		1 m LiDAR DEM		2 m LiDAR DEM	
Average point density (m^{-2})	Average point spacing (m)	Reduction in point density (%)	Catchment	Hedgerow banks	Catchment	Hedgerow banks	Catchment	Hedgerow banks	Catchment	Hedgerow banks
40.2	0.16	0	–	–	–	–	–	–	–	–
5	0.45	87.56	0.02	0.04	0.02	0.03	3.04	0.48	2.11	0.68
2	0.71	95.02	0.02	0.09	0.02	0.08	3.05	0.94	2.11	0.82
1	1	97.51	0.03	0.19	0.03	0.16	3.07	1.44	2.23	1.23
0.5	1.41	98.76	0.04	0.34	0.04	0.29	3.07	1.81	2.26	1.82
0.25	2	99.38	0.05	0.53	0.05	0.47	5.08	2.28	5.13	2.08
0.125	2.83	99.69	0.06	0.65	0.06	0.59	5.30	2.50	5.32	2.36
0.0156	8	99.96	0.09	0.79	0.09	0.73	5.38	3.12	5.44	2.92

Another important consideration when modelling HSAs is accounting for the effects of flow sinks. TWI maps were derived from hydrologically corrected, depressionless DEMs which removed flow sinks, including at field boundaries, in order to model hydrologically connected flow pathways to the catchment outlet. This is a necessary DEM pre-processing stage and the requirement is particularly acute when using high resolution LiDAR DEMs due to their ability to capture fine-scale sinks. However, field observations indicated that flow sinks, particularly at field boundaries, were a common microtopographic feature impeding and attenuating water (and potentially pollutants) (Supplementary Fig. S3 in the online cersion at DOI: http://dx.doi.org/10.1016/j.jag.2016.08.012). A solution could be to create flow sink maps, by subtracting elevations of the unfilled DEM version from the filled DEM (Fink and

Drohan, 2016), and calculate flow sink overland flow volume capacities. These flow sink maps could then be overlaid onto modelled HSAs to estimate the existing likelihood of hydrological disconnection and mitigation of pollutant transport pathways (see Thomas et al., 2016). As flow sinks are often very fine-scale and subtle features, sub-metre resolution DEMs may be optimal for this particular task.

5. Conclusions

This study identified 1–2 m resolution DEMs as optimal for modelling HSAs (runoff generating areas) in complex agricultural catchments dominated by microtopographic features based on TWI thresholds. These resolutions were able to balance the need to model both microtopographic influences on surface runoff pathways and the hillslope scale convergence of flow. As conventional and proprietary 5 m DEMs were unable to capture microtopography, modelled HSAs were much less accurate (10–84% compared to 70–100% with 1–2 m LiDAR DEMs when evaluated using field observations). LiDAR DEMs at 0.25 m resolution were also found to be unsuitable for defining surface runoff propensity due to the effects of very high topographic detail and small grid size on slope and flow accumulation, and were required to be resampled to coarser resolutions. The optimal DEMs were able to predict critical breakthrough and delivery points along surface runoff pathways where mobilised pollutants could potentially be transported between fields or delivered to the drainage channel network. This could allow the onward targeting of HSA and CSA mitigation measures and best management practices at sub-field scales to reduce diffuse pollution. The study also found that initial LiDAR bare-earth point densities could be significantly reduced, as little loss of vertical accuracy was found in 1–2 m LiDAR DEMs with 2–5 points m^{-2}, even at hedgerow bank features. However, further work is needed to assess vertical accuracies of other microtopographic features following point thinning of DEMs. Furthermore, soil hydrological properties should be incorporated in HSA definitions as runoff propensity was over-predicted in upper hillslope positions (where well drained soils dominate) as shown by field observations. Optimal DEM resolutions for defining microtopographic flow sinks will also need to be considered as these were observed to be important flow attenuating features but were removed during standard hydrological correction of DEMs.

Acknowledgements

This research is part of the Agricultural Catchments Programme (ACP), funded by the Irish Department of Agriculture, Food and the Marine (DAFM) and the Teagasc Walsh Fellowship Scheme (DAFM 6300). We thank ACP farmers for cooperation and access to their land, the ACP team and staff at the Teagasc Environment, Soils and Land Use Department, Johnstown Castle, Wexford, Ireland. We also thank the Irish DAFM for discussions on the applicability of topographic indices within policy, and acknowledge FugroBKS Ltd, Coleraine, N. Ireland, for acquisition of the LiDAR data.

References

Ågren, A.M., Lidberg, W., Strömgren, M., Ogilvie, J., Arp, P.A., 2014. Evaluating digital terrain indices for soil wetness mapping —a Swedish case study. Hydrol. Earth Syst. Sci. 11, 4103–4129.

Agnew, L.J., Lyon, S., Gerard-Marchant, P., Collins, V.B., Lembo, A.J., Steenhuis, T.S., Walter, M.T., 2006. Identifying hydrologically sensitive areas: bridging the gap between science and application. J. Environ. Manage. 78, 63–76.

Ali, G., Birkel, C., Tetzlaff, D., Soulsby, C., McDonnell, J.J., Tarolli, P., 2014. A comparison of wetness indices for the prediction of observed connected saturated areas under contrasting conditions. Earth Surf. Proc. Landf. 39, 399–413.

Anderson, E.S., Thompson, J.A., Crouse, D.A., Austin, R.E., 2006. Horizontal resolution and data density effects on remotely sensed LIDAR-based DEM. Geoderma 132, 406–415.

Beven, K.J., Kirkby, M.J., 1979. A physically based: variable contributing area model of basin hydrology. Hydrol. Sci. Bull. 24, 43–69.

Beven, K., 2001. How far can we go in distributed hydrological modelling? Hydrol. Earth Syst. Sci. 5, 1–12.

Blyth, E., Finch, J., Robinson, M., Rosier, P., 2004. Can soil moisture be mapped onto the terrain? Hydrol. Earth Syst. Sci. Discuss. 8, 923–930.

Bracken, L.J., Croke, J., 2007. The concept of hydrological connectivity and its contribution to understanding runoff-dominated geomorphic systems. Hydrol. Processes 21, 1749–1763.

Brubaker, K.M., Myers, W.L., Drohan, P.J., Miller, D.A., Boyer, E.W., 2013. The use of lidar terrain data in characterizing surface roughness and microtopography. Appl. Environ. Soil Sci. 2013.

Buchanan, B.P., Falbo, K., Schneider, R.L., Easton, Z.M., Walter, M.T., 2013a. Hydrological impact of roadside ditches in an agricultural watershed in Central New York: implications for non-point source pollutant transport. Hydrol. Processes 27, 2422–2437.

Buchanan, B.P., Archibald, J.A., Easton, Z.M., Shaw, S.B., Schneider, R.L., Walter, T.M., 2013b. A phosphorus index that combines critical source areas and transport pathways using a travel time approach. J. Hydrol. 486, 123–135.

Buchanan, B.P., Fleming, M., Schneider, R.L., Richards, B.K., Archibald, J., Qiu, Z., Walter, M.T.1, 2014. Evaluating topographic wetness indices across central New York agricultural landscapes. Hydrol. Earth Syst. Sci. 18, 3279–3299.

Chang, K.-T., Tsai, B.-W., 1991. The effect of DEM resolution on slope and aspect mapping. Cartogr. Geogr. Inf. Syst. 18, 69–77.

Djodjic, F., Villa, A., 2015. Distributed: high-resolution modelling of critical source areas for erosion and phosphorus losses. Ambio 44, 241–251.

Doody, D.G., Archbold, M., Foy, R.H., Flynn, R., 2012. Approaches to the implementation of the Water Framework Directive: targeting mitigation measures at critical source areas of diffuse phosphorus in Irish catchments. J. Environ. Manage. 93, 225–234.

Drover, D.R., Jackson, C.R., Bitew, M., Du, E.1, 2015. Effects of DEM scale on the spatial distribution of the TOPMODEL topographic wetness index and its correlations to watershed characteristics. Hydrol. Earth Syst. Sci. Discuss. 2015, 11817–11846.

Duke, G.D., Kienzle, S.W., Johnson, D.L., Byrne, J.M., 2003. Improving overland flow routing by incorporating ancillary road data into digital elevation models. J. Spatial Hydrol., 3.

Fink, C.M., Drohan, P.J., 2016. High resolution hydric soil mapping using LiDAR digital terrain modeling. Soil Sci. Soc. Am. J. 80, 355–363.

Galzki, J.C., Birr, A.S., Mulla, D.J., 2011. Identifying critical agricultural areas with three-meter LiDAR elevation data for precision conservation. J. Soil Water Conserv. 66, 423–430.

Gburek, W.J., Sharpley, A.N., 1998. Hydrologic controls on phosphorus loss from Upland agricultural watersheds. J. Environ. Qual. 27, 267–277.

Gillin, C.P., Bailey, S.W., McGuire, K.J., Prisley, S.P., 2015. Evaluation of LiDAR-derived DEMs through terrain analysis and field comparison. Photogramm. Eng. Remote Sens. 81, 387–396.

Hancock, G.R., 2005. The use of digital elevation models in the identification and characterization of catchments over different grid scales. Hydrol. Processes 19, 1727–1749.

Heathwaite, A.L., Quinn, P.F., Hewett, C.J.M.1, 2005. Modelling and managing critical source areas of diffuse pollution from agricultural land using flow connectivity simulation. J. Hydrol. 304, 446–461.

Hengl, T., 2006. Finding the right pixel size. Comput. Geosci. 32, 1283–1298.

Jordan, P., Melland, A.R., Mellander, P.E., Shortle, G., Wall, D., 2012. The seasonality of phosphorus transfers from land to water: implications for trophic impacts and policy evaluation. Sci. Total Environ. 434, 101–109.

Kienzle, S., 2004. The effect of DEM raster resolution on first order: second order and compound terrain derivatives. Trans. GIS 8, 83–111.

Kuo, W.L., Steenhuis, T.S., McCulloch, C.E., Mohler, C.L., Weinstein, D.A., DeGloria, S.D., Swaney, D.P., 1999. Effect of grid size on runoff and soil moisture for a variable-source-area hydrology model. Water Resour. Res. 35, 3419–3428.

Lane, S.N., Reaney, S.M., Heathwaite, A.L., 2009. Representation of landscape hydrological connectivity using a topographically driven surface flow index. Water Resour. Res. 45, W08423.

Liu, X., Zhang, Z., 2008. LiDAR data reduction for efficient and high quality DEM generation. International Archives of the Photogrammetry. Remote Sens. Spatial Inf. Sci. 37, 173–178.

Liu, X., 2008. Airborne LiDAR for DEM generation: some critical issues. Prog. Phys. Geogr. 32, 31–49.

Luscombe, D.J., Anderson, K., Gatis, N., Wetherelt, A., Grand-Clement, E., Brazier, R.E., 2015. What does airborne LiDAR really measure in upland ecosystems? Ecohydrology 8, 584–594.

Lyon, S.W., Walter, M.T., Gérard-Marchant, P., Steenhuis, T.S., 2004. Using a topographic index to distribute variable source area runoff predicted with the SCS curve-number equation. Hydrol. Processes 18, 2757–2771.

MacMillan, R.A., Martin, T.C., Earle, T.J., McNabb, D.H.1, 2003. Automated analysis and classification of landforms using high-resolution digital elevation data: applications and issues. Can. J. Remote Sens. 29, 592–606.

Marjerison, R.D., Dahlke, H., Easton, Z.M., Seifert, S., Walter, M.T., 2011. A Phosphorus Index transport factor based on variable source area hydrology for New York State. J. Soil Water Conserv. 66, 149–157.

Melland, A.R., Mellander, P.E., Murphy, P.N.C., Wall, D.P., Mechan, S., Shine, O., Shortle, G., Jordan, P., 2012. Stream water quality in intensive cereal cropping catchments with regulated nutrient management. Environ. Sci. Policy 24, 58–70.
Mellander, P.-E., Melland, A.R., Jordan, P., Wall, D.P., Murphy, P.N.C., Shortle, G., 2012. Quantifying nutrient transfer pathways in agricultural catchments using high temporal resolution data. Environ. Sci. Policy 24, 44–57.
Mellander, P.E., Jordan, P., Shore, M., Melland, A.R., Shortle, G., 2015. Flow paths and phosphorus transfer pathways in two agricultural streams with contrasting flow controls. Hydrol. Processes, http://dx.doi.org/10.1002/hyp.10415.
Moore, I.D., Grayson, R.B., Ladson, A.R., 1991. Digital terrain modelling: a review of hydrological, geomorphological: and biological applications. Hydrol. Processes 5, 3–30.
Murphy, P.N.C., Ogilvie, J., Meng, F., Arp, P.A., 2008. Stream network modelling using lidar and photogrammetric digital elevation models: a comparison and field verification. Hydrol. Processes 22, 1747–1754.
Murphy, P.N.C., Ogilvie, J., Arp, P., 2009. Topographic modelling of soil moisture conditions: a comparison and verification of two models. Eur. J. Soil Sci. 60, 94–109.
Page, T., Haygarth, P.M., Beven, K.J., Joynes, A., Butler, T., Keeler, C., Freer, J., Owens, P.N., Wood, G.A., 2005. Spatial variability of soil phosphorus in relation to the topographic index and critical source areas. J. Environ. Qual. 34, 2263–2277.
Pionke, H.B., Gburek, W.J., Sharpley, A.N., 2000. Critical source area controls on water quality in an agricultural watershed located in the Chesapeake Basin. Ecol. Eng. 14, 325–335.
Quinn, P., Beven, K., Chevallier, P., Planchon, O., 1991. The prediction of hillslope flow paths for distributed hydrological modelling using digital terrain models. Hydrol. Processes 5, 59–79.
Raber, G.T., Jensen, J.R., Hodgson, M.E., Tullis, J.A., Davis, B.A., Berglund, J.1, 2007. Impact of LiDAR nominal post-spacing on DEM accuracy and flood zone delineation. Photogramm. Eng. Remote Sens. 73, 793–804.
Sørensen, R., Seibert, J., 2007. Effects of DEM resolution on the calculation of topographical indices: TWI and its components. J. Hydrol. 347, 79–89.
Schneiderman, E.M., Steenhuis, T.S., Thongs, D.J., Easton, Z.M., Zion, M.S., Neal, A.L., Mendoza, G.F., Walter, T.M., 2007. Incorporating variable source area hydrology into a curve-number-based watershed model. Hydrol. Process. 21, 3420–3430.
Sharpley, A., Foy, B., Withers, P., 2000. Practical and innovative measures for the control of agricultural phosphorus losses to water: an overview. J. Environ. Qual. 29, 1–9.
Sharpley, A., Kleinman, P., McDowell, R., Gitau, M., Bryant, R., 2002. Modeling phosphorus transport in agricultural watersheds: processes and possibilities. J. Soil Water Conserv. 57, 425–439.
Sharpley, A., Kleinman, P., Flaten, D., Buda, A., 2011. Critical source area management of agricultural phosphorus: experiences: challenges and opportunities. Water Sci. Technol. 64, 945–952.
Sharpley, A., Berström, L., Aronsson, H., Bechmann, M., Bolster, C., Börling, K., Djodjic, F., Jarvie, H., Schoumans, O., Stamm, C., 2015. Future agriculture with minimized phosphorus losses to waters: research needs and direction. Ambio 44, 163–179.
Sherriff, S.C., Rowan, J.S., Melland, A.R., Jordan, P., Fenton, O., Ó Huallacháin, D., 2015. Investigating suspended sediment dynamics in contrasting agricultural catchments using ex situ turbidity-based suspended sediment monitoring. Hydrol. Earth Syst. Sci. 19, 3349–3363.
Shore, M., Murphy, P.N.C., Jordan, P., Mellander, P.E., Kelly-Quinn, M., Cushen, M., Mechan, S., Shine, O., Melland, A.R.1, 2013. Evaluation of a surface hydrological connectivity index in agricultural catchments. Environ. Modell. Softw. 47, 7–15.
Shore, M., Jordan, P., Mellander, P.E., Kelly-Quinn, M., Wall, D.P., Murphy, P.N.C., Melland, A.R., 2014. Evaluating the critical source area concept of phosphorus loss from soils to water-bodies in agricultural catchments. Sci. Total Environ. 490, 405–415.
Sonneveld, M.P.W., Schoorl, J.M., Veldkamp, A., 2006. Mapping hydrological pathways of phosphorus transfer in apparently homogeneous landscapes using a high-resolution DEM. Geoderma 133, 32–42.
Srinivasan, M.S., Mcdowell, R.W., 2009. Identifying critical source areas for water quality: 1. Mapping and validating transport areas in three headwater catchments in Otago, New Zealand. J. Hydrol. 379, 54–67.
Tarboton, D.G.1, 1997. A new method for the determination of flow directions and upslope areas in grid digital elevation models. Water Resour. Res. 33, 309–319.
Tenenbaum, D., Band, L., Kenworthy, S., Tague, C., 2006. Analysis of soil moisture patterns in forested and suburban catchments in Baltimore, Maryland, using high-resolution photogrammetric and LIDAR digital elevation datasets. Hydrol. Process. 20, 219–240.
Thomas, I.A., Jordan, P., Mellander, P.-E., Fenton, O., Shine, O., Ó Huallacháin, D., Creamer, R., McDonald, N.T., Dunlop, P., Murphy, P.N.C., 2016. Improving the identification of hydrologically sensitive areas using LiDAR DEMs for the delineation and mitigation of critical source areas of diffuse pollution. Sci. Total Environ. 556, 276–290.
Thompson, J.A., Bell, J.C., Butler, C.A., 2001. Digital elevation model resolution: effects on terrain attribute calculation and quantitative soil-landscape modeling. Geoderma 100, 67–89.
Vaze, J., Teng, J., Spencer, G., 2010. Impact of DEM accuracy and resolution on topographic indices. Environ. Modell. Softw. 25, 1086–1098.
Wall, D., Jordan, P., Melland, A.R., Mellander, P.E., Buckley, C., Reaney, S.M., Shortle, G., 2011. Using the nutrient transfer continuum concept to evaluate the european union nitrates directive national action programme. Environ. Sci. Policy 14, 664–674.
Walter, M.T., Walter, M.F., Brooks, E.S., Steenhuis, T.S., Boll, J., Weiler, K., 2000. Hydrologically sensitive areas: variable source area hydrology implications for water quality risk assessment. J. Soil Water Conserv. 55, 277–284.
Walter, M.T., Steenhuis, T.S., Mehta, V.K., Thongs, D., Zion, M., Schneiderman, E., 2002. Refined conceptualization of TOPMODEL for shallow subsurface flows. Hydrol. Processes 16, 2041–2046.
Wang, L., Liu, H., 2006. An efficient method for identifying and filling surface depressions in digital elevation models for hydrologic analysis and modelling. Int. J. Geogr. Inf. Sci. 20, 193–213.
Wolock, D.M., Price, C.V., 1994. Effects of digital elevation model map scale and data resolution on a topography-based watershed model. Water Resour. Res. 30, 3041–3052.
Wu, S., Li, J., Huang, G.H., 2008. A study on DEM-derived primary topographic attributes for hydrologic applications: sensitivity to elevation data resolution. Appl. Geogr. 28, 210–223.
Zevenbergen, L.W., Thorne, C.R., 1987. Quantitative analysis of land surface topography. Earth Surf. Processes Landf. 12, 47–56.
Zhang, W., Montgomery, D.R., 1994. Digital elevation model grid size, landscape representation, and hydrologic simulations. Water Resour. Res. 30, 1019–1028.